Quantum Electronics **30** (9) 753 – 766 (2000)

INVITED PAPER

PACS numbers: 42.65.Ky; 42.70.Mp
DOI: 10.1070/QE2000v030n09ABEH001810

Frequency conversion of Bessel light beams in nonlinear crystals

V N Belyi, N S Kasak, N A Khilo

Abstract. The properties of frequency conversion of Bessel light beams (BLBs) in nonlinear crystals are studied theoretically and experimentally. New possibilities and prospects of the development of methods for nonlinear optical frequency conversion using BLBs are discussed. The second harmonic generation (SHG) is studied under the conditions of critical and noncritical phase matching. The longitudinal and transverse phase matching is analysed in detail upon SHG and sum frequency generation in BLBs. The concept of azimuthal width of phase matching caused by the longitudinal and transverse wave detuning is introduced, and its value is calculated for collinear and π-vector interactions. The regime of azimuthally matched interactions is selected, which is realised when the azimuthal phase matching width is small. A correlation of the azimuthal BLB components caused by these interactions is predicted. It is shown that azimuthally matched BLBs are characterised by a significant increase in the overlap integral and by nonlinear interactions that do not destroy their spatial structure.

1. Introduction

The study of Bessel light beams (BLBs) has been initiated quite recently [1 – 4]. Initially, they attracted attention due to their so-called raylike property [1]. This property lies in the fact that a change in the amplitude-phase profile of a BLB propagating in a free space is caused only by its finite transverse size. For this reason, the near-axis part of the beam experiences minimal diffraction distortions. Moreover, a screening of the central region of the BLB produces a compensating radial energy flux, which restores the transverse profile of the beam. These specific features of the BLB are unique and they can be used in various fields of optics, spectroscopy, laser physics, and for studying the interaction of light with a matter.

In the last years, nonlinear optics of BLBs has been extensively developed [5 – 22]. At present, many known nonlinear optical effects, which have been earlier investigated for Gaussian beams, were observed using BLBs. The self-interaction [5], generation of the second [6 – 8, 19, 21] and third [9 – 11, 15] harmonics, SRS [12, 16, 17], and parametric frequency conversion of light [13, 14, 18, 20, 22] have been investigated. It has been shown that the main feature of the nonlinear optical frequency conversion of Bessel beams is a dominant role of vector interactions. This feature follows from the structure of the spectrum of spatial frequencies of the BLB, which represents, as is known, a circular cone in the wave vector space.

Despite quite extensive studies of frequency conversion of BLBs, some important questions concerning the advantages of BLBs and their future applications remain unclear. These issues are especially urgent because nonlinear optical frequency converters available at present, which use Gaussian and super-Gaussian laser beams, are quite diversified, highly efficient, and reliable. The aim of this paper is not only to generalise the results concerning the features of frequency conversion of BLBs but also to reveal new possibilities and prospects of nonlinear optics of Bessel beams.

2. Longitudinal phase matching in three-frequency interaction of Bessel beams

In the case of BLBs, in contrast to Gaussian beams, not only collinear but various vector interactions within cones of the wave vectors of the beams can be involved in nonlinear optical processes. However, in the general case, different vector interactions have different efficiency. The efficiency is limited by a number of factors, the first one being the fulfilment of the condition of longitudinal phase matching.

Consider the wave detuning $\Delta k_z = k_{2ez} - k_{1oz} - k_{1ez}$ (Fig. 1a) in the general case of the three-wave oe-e interaction of

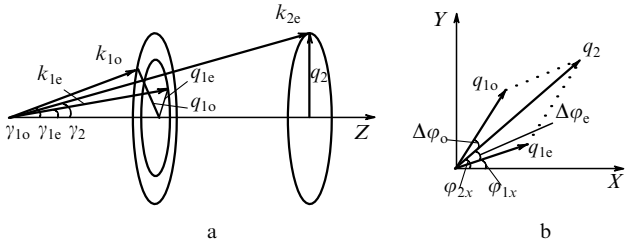

Figure 1. Geometry of the three-wave mixing of BLBs (a) and phase matching of the transverse components of the wave vectors (b). The Z-axis is located either in the principal plane of a uniaxial crystal or in one of the three principal planes of a biaxial crystal.

V N Belyi, N S. Kazak B I Stepanov Institute of Physics, National Academy of Sciences of Belarus, prosp. Skoriny 70, 220072 Minsk, Belarus
N A Khilo Division of Optical Problems in Information Technologies, National Academy of Sciences of Belarus, ul. Kuprevicha 1, k. 2, 220141 Minsk, Belarus. E-mail: nkhilo@optoinform.bas-net.by

Received 21 January 2000; revision received 10 May 2000
Kvantovaya Elektronika **30** (9) 753 – 766 (2000)
Translated by M N Sapozhnikov

type II in a uniaxial crystal or in a principal plane of a biaxial crystal. By expanding the longitudinal components $k_{1o,ez}$ and k_{2ez} of the wave vectors in a series over small transverse components q_m, we obtain, under the conditions of critical phase matching, the following expression for Δk_z:

$$\Delta k_z \approx \Delta k_G + \beta_2 q_{2x} - \beta_1 q_{1ex} - \frac{q_2^2}{2k_{2e}} + \frac{q_{1o}^2}{2k_{1o}} + \frac{q_{1e}^2}{2k_{1e}}, \quad (1)$$

where $\Delta k_G = k_{2e} - k_{1o} - k_{1e}$ is the wave detuning for Gaussian beams propagating along the BLB axis; $\beta_1 = \partial k_{1ez}/\partial q_{1ex}$, and $\beta_2 = \partial k_{2ez}/\partial q_{2ex}$ are birefringence angles; q_2 is the BLB conicity parameter at the double frequency. Hereafter, we will call the transverse components q_m the BLB conicity parameters. To correctly describe the three-wave interaction, it is necessary to introduce detuning also for transverse components (see section 5 and Fig. 1b):

$$\Delta q = q_2 - q_{1o}\cos\Delta\varphi_o - q_{1e}\cos\Delta\varphi_e. \quad (2)$$

In the case of SHG by Bessel beams with the same conicity parameters q_1, expressions (1) and (2) will take the form

$$\Delta k_z \approx \Delta k_G + \beta_2 q_{2x} - \beta_1 q_{1x} - \frac{q_2^2}{2k_{2e}} + \frac{q_1^2}{k_{1o}}, \quad (3)$$

$$\Delta q = q_2 - 2q_1\cos\Delta\varphi. \quad (4)$$

Thus, for $\Delta\varphi = 0$ and $\Delta q = 0$, the collinear phase matching is realised and the relation $q_2 = 2q_1$ takes place. For $\Delta\varphi = \pi/2$, the vector phase matching of the oppositely oriented plane-wave BLB components (π phase matching) is realised and $q_2 \approx 0$. When $0 < \Delta\varphi < \pi/2$, a variety of types of vector phase matching is realised.

By introducing the BLB conicity angles γ_m by means of the relations $\sin\gamma_{1o,e} = q_{1o,e}/k_{1o,e}$ and $\sin\gamma_2 = q_2/k_{2e}$ and assuming these angles to be small, we obtain from (4) for $\Delta q = 0$

$$\Delta k_z \approx \Delta k_G - k_{1o}\left[\gamma_2^2 - {}^1\!/_2(\gamma_{1o}^2 + \gamma_{1e}^2)\right.$$

$$\left. + \beta_1\gamma_{1e}\cos\varphi_{1x} - 2\beta_2\gamma_2\cos\varphi_{2x}\right]. \quad (5)$$

Expression (5) describes the wave detuning as a function of azimuthal angles φ_{1x} and $\varphi_{2x}$of the plane-wave BLB components at the fundamental frequency and the second harmonic (Fig. 1b). These angles are not independent but related by the expression $\varphi_{2x} = \varphi_{1x} + \Delta\varphi_e$ (Fig. 1b). For the collinear phase matching, $\Delta\varphi_o = \Delta\varphi_e = 0$, and for π phase matching, $\Delta\varphi_o + \Delta\varphi_e = \pi$. The ultimate detuning (5) for collinear and π phase matching are realised when $\varphi_{1,2x} = 0$ and 180°:

$$\Delta k_{z\,coll}^{\pm} = \Delta k_G \pm \gamma_1 k_{1o}(2\beta_2 - \beta_1), \quad (6)$$

$$\Delta k_{z\,vect}^{\pm} = \Delta k_G + k_{1o}\gamma_1^2 \pm k_{1o}\gamma_1\beta_1. \quad (7)$$

One can see from expressions (6) and (7) that the range of variation of the wave detuning is determined by the anisotropy angles $\beta_{1,2}$ and also depends on the parameter Δk_G.

Thus, the wave detuning in an anisotropic crystal depends on the azimuth. The azimuthal dependence of detuning results in the general case in the violation of a cylindrical symmetry of the distribution of the second-harmonic intensity. This is important first of all for the interaction of the collinear type at which the SHG of BLBs is possible.

The coherent lengths for linear and π-vector interactions can be calculated from the known wave detuning from the condition $\Delta k_z^{\pm} L = \pm\pi$ as

$$L_{coll}^{\pm} = \frac{\pi}{|\Delta k_G \pm \gamma_1 k_{1o}(2\beta_2 - \beta_1)|},$$

$$L_{vect}^{\pm} = \frac{\pi}{|\Delta k_G + \gamma_1 k_{1o}(\gamma_1 \pm \beta_1)|}. \quad (8)$$

It follows from (8) that to achieve the maximum coherent length in the case of collinear interaction, one should set $\Delta k_G = 0$. At the same time, for the vector interaction, the choice of the nonzero detuning Δk_G is optimal.

As an example, consider the numerical estimate of the coherent lengths for SHG in a Nd:YAG laser in a KTP crystal, for which $\beta_1 \approx 0.202°$ and $\beta_2 \approx -0.268°$ [23]. Assuming the conicity angle of a BLB at the fundamental frequency outside the crystal to be 1°, we obtain $L_{coll} \approx 5$ mm for $\Delta k_G = 0$. To increase the coherent length in the case of π phase matching, we should set $\Delta k_G = 0.4\ \text{mm}^{-1}$. In this case, the minimum length L_{vect} proves to be equal to ~ 3 mm and the minimum length L_{coll} is also equal to ~ 3 mm. Therefore, in a KTP crystal of thickness ~ 3 mm, both collinear and π-interactions will occur within the angular width of the longitudinal phase matching. In a crystal of a greater thickness, the axial symmetry of the interaction can be achieved, as follows from (8), by decreasing the conicity angle γ_1.

The coherent length (8) also depends on the interaction type. For the oo-e interaction in uniaxial crystals, one should set $\beta_1 = 0$ in expressions (8). In this case the π-vector interaction proves to be axially symmetric, whereas the collinear interaction will be, as before, inhomogeneous in the azimuth. In strongly anisotropic crystals, such as BBO, for which $\beta_2 = -3.187°$ [23], the coherent length L_{coll} is small, and to increase it, the conicity parameter γ_1 should be decreased in a proper way.

Consider now the SHG for Bessel beams propagating in the direction of noncritical phase matching. In particular, for uniaxial crystals, this is the direction of the 90° phase matching, while for biaxial crystals – the direction coinciding with crystallographic axes. As an example, consider the type I interaction in a $KNbO_3$ crystal having the symmetry *mm*2. A BLB at the fundamental frequency polarised along the direction $X_2 \,||\, \boldsymbol{a}$ propagates along the axis $X_2 \,||\, \boldsymbol{b}$ and excites the second harmonic with polarisation directed along the X_3-axis (Fig. 2). At room temperature (22 °C), such phase matching takes place near a wavelength of 982 nm, and at 181 °C, at 1.064 nm [24].

For small angles γ in the vicinity of the X_1-axis, the refractive indices of the fast (N_+) and slow (N_-) waves have the form

$$N_+(\varphi_1) = N_3 + \gamma^2\delta_{13}\sin^2\varphi_1,$$

$$N_-(\varphi_1) = N_2 + \gamma^2\delta_{12}\cos^2\varphi_1, \quad (9)$$

where $\delta_{13} = N_3^3(N_3^{-2} - N_1^{-2})/2$, and $\delta_{12} = N_2^3(N_2^{-2} - N_1^{-2})/2$; $N_{1,2,3}$ are the principal refractive indices of a $KnbO_3$ crystal along crystal optic axes X_1, X_2, and X_3 (Fig. 2). Because $N_1 > N_2 > N_3$, we have $\delta_{12} > 0$ and $\delta_{13} > 0$.

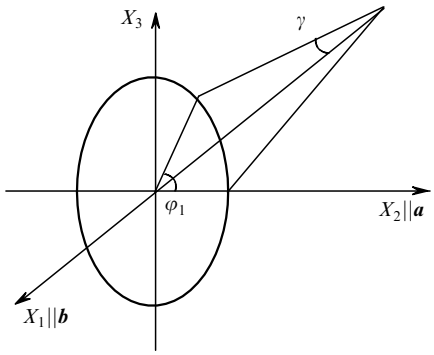

Figure 2. Orientation of the BLB at the fundamental frequency in a scheme of noncritical phase matching upon the SHG.

The phase matching condition for the type I collinear interaction, when the slow wave at the fundamental frequency excites the second-harmonic fast wave, taking into account (9), has the form

$$\Delta k_z(\lambda, \varphi_1) = \Delta k_G(\lambda) + 2k_0\gamma^2 \times [\delta_{13}(\lambda)\sin^2\varphi_1 - \delta_{12}(\lambda)\cos^2\varphi_1], \quad (10)$$

where $\Delta k_G(\lambda) = 2k_0[N_3(\lambda/2) - N_2(\lambda)]$. Expression (10) allows one to determine the wave detuning for any azimuthal angle φ_1 within the wave vector cone for BLBs. The type of the azimuthal dependence Δk_z strongly depends on the sign of detuning Δk_G for a Gaussian beam. In the wavelength region where $\Delta k_G > 0$, the maximum detuning is achieved for $\varphi_1 = \pi/2$. For $\Delta k_G < 0$, the detuning is maximum at $\varphi_1 = 0$.

For $KNbO_3$ at room temperature, we have, according to the Sellmeyer formulas [23], $\Delta k_G = 0$ at the wavelength $\lambda_{10} = 982.1$ nm. In this case, for $\lambda < \lambda_{10}$, the detuning Δk_G is positive, while for $\lambda > \lambda_{10}$, it is negative. In the wavelength region $\lambda < \lambda_{10}$, the minimum coherence length corresponding to the angle $\varphi_1 = \pi/2$ is $L_{left} = \lambda/4|N_3(\lambda/2) - N_2(\lambda) + \gamma^2\delta_{13}|$; for $\lambda > \lambda_{10}$, the minimum coherence length $L_{right} = \lambda/4|N_3(\lambda/2) - N_2(\lambda) - \gamma^2\delta_{12}|$ corresponds to the angle $\varphi_0 = 0$. Fig. 3 shows the dependences of coherence lengths on λ in the vicinity $\lambda = \lambda_{10}$. One can see that L_{coh} rapidly decreases with increasing wavelength detuning from λ_{10}. For example, the inequality $L_{coh} > 3$ mm takes place in the wavelength range $981.76 < \lambda < 982.34$ nm.

Therefore, in a given interval of width ~ 0.7 nm, the collinear phase matching is realised for all azimuthal angles. The generation of an azimuthally homogeneous second-harmonic field outside this range becomes impossible.

A similar consideration can be performed, for example, for a LBO crystal, for which $N_1 < N_2 < N_3$ in a system of crystal optic axes $X_1 \,||\, \boldsymbol{a}, X_2 \,||\, \boldsymbol{c}, X_3 \,||\, \boldsymbol{b}$. A fundamental frequency BLB linearly polarised along the X_3-axis and propagating along the X_2-axis will generate a second-harmonic BLB polarised along the X_1-axis. The type I phase matching will be satisfied at room temperature at the wavelength about 551 nm [23]. The wave detuning can be calculated from expressions (9) and (10) by making replacements $N_3 \to N_1$, $N_1 \to N_2$, and $N_2 \to N_3$.

Finally, the noncritical phase matching for Bessel beams in uniaxial crystals is realised upon their propagation along the direction of the 90° phase synchronism. To find the wave detuning in this case, one should set $\delta_{12} = 0, \delta_{13} = N_e^3(N_e^{-2} - N_o^{-2})/2$ in (9) and (10), and to measure the angle φ_1 from the optic axis direction.

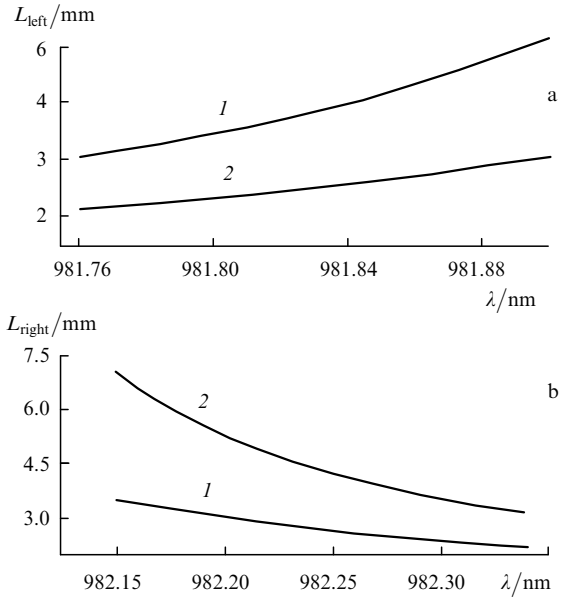

Figure 3. Dependences of the coherent lengths L_{left} (a) and L_{right} (b) on the wave length for a $KnbO_3$ crystal for the conicity angle $\gamma_1 = 1$ (*1*) and 2° (*2*).

3. The azimuthal width of phase matching for collinear and vector interactions

Along with known characteristics of the SHG in Gaussian light beams such as the angular and spectral width of phase matching, the azimuthal width of phase matching plays an important role in nonlinear optics of BLBs. The necessity of introducing this SHG characteristic is explained by the fact that the change $\delta\varphi$ in the azimuthal angle between the interacting plane-wave BLB components (Fig. 1) results in a change in the wave detuning $\Delta k_z(\delta\varphi)$.

Let us calculate the azimuthal width of phase matching for SHG. Consider first the interaction under conditions close to the collinear phase matching. The geometrical parameters of the problem correspond to Fig. 1 if we set $\Delta\varphi_{o,e} = \delta\varphi$ and $\varphi_{2x} = \varphi_2$. The longitudinal wave detuning and the transverse phase matching condition can be written in the form

$$\Delta k_z(\varphi_2, \delta\varphi) = 2k_0 N_{+2}(\gamma_2, \varphi_2)\cos\gamma_2 - k_0[N_{-1}(\gamma_1, \varphi_2 - \delta\varphi) + N_{-1}(\gamma_1, \varphi_2 + \delta\varphi)]\cos\gamma_1, \quad (11)$$

$$2N_{+2}(\gamma_2, \varphi_2)\sin\gamma_2 - [N_{-1}(\gamma_1, \varphi_2 - \delta\varphi) + N_{-1}(\gamma_1, \varphi_2 + \delta\varphi)]\cos\delta\varphi\sin\gamma_1 = 0, \quad (12)$$

where $N_{+2} = N_+(2\omega)$; $N_{-1} = N_-(\omega)$; and $N_\pm$ are given by expressions (9).

The expansion of (11) and (12) in the vicinity of the azimuthal angle of the second harmonic $\varphi = \varphi_2$ at the fixed angle γ_1 gives Δk_z as a function of φ_2 and $\delta\varphi$ in the form

$$\Delta k_z(\varphi_2, \delta\varphi) \approx \Delta k_z(\varphi_2) + k_0 N_2 \gamma_1^2 (\delta\varphi)^2, \quad (13)$$

where $\Delta k_z(\varphi_2)$ is defined by expression (10); γ_1 is the BLB conicity angle outside a crystal. Expression (13) relates the wave detuning to the average azimuthal angle φ_2 of each pair of the plane-wave BLB components and the angle $\delta\varphi$ between them. One can see that the contribution to the wave detuning caused by the nonzero value of $\delta\varphi$ is always positive, so that the behaviour of the total detuning in (13) will strongly depend on the sign of $\Delta k_z(\varphi_2)$.

As shown above for a $KNbO_3$ crystal, the sign of the function $\Delta k_z(\varphi_2)$ depends on the wavelength. For this reason, vector interactions with $\delta\varphi \neq 0$ will increase detuning in the wavelength region where $\Delta k_z(\varphi_2)$ is positive. Therefore, in this case, the maximum value of $\delta\varphi$ will be restricted, as a rule, by the condition of longitudinal phase matching. When $\Delta k_z(\varphi_2)$ is negative, interactions with $\delta\varphi \neq 0$ will decrease the detuning. In this case, the maximum value of $\delta\varphi$ will be restricted by the condition of transverse phase matching (see also section 5).

By setting $\Delta k_z L = \pi$ in (13), we obtain the expression for the azimuthal half-width $\delta\varphi_{\rm coll}$, which corresponds to collinear interactions

$$\delta\varphi_{\rm coll} = \frac{1}{\gamma_1\sqrt{N_2}}\left(\frac{\lambda_1}{2L} - \frac{\Delta k_z(\varphi_2)}{k_0}\right)^{1/2}. \qquad (14)$$

Expression (14) allows one to determine the maximum angle between the plane-wave BLB components generating the second harmonic within the angular width of phase matching. This expression shows that vibrational phase matching is noncritical with respect to the azimuthal angle. In the wavelength region where the longitudinal detuning is nonnegative, the maximum angle $\delta\varphi_{\rm coll}$ is realised for $\Delta k_z = 0$. The numerical estimate with parameters $L = 1$ cm, $\gamma_1 = 2^\circ$, and $N_2 = 2.25$ gives, according to (14), $\delta\varphi_{\rm coll} \approx 8^\circ$.

The azimuthal half-width $\delta\varphi_{\rm vect}$ of phase matching for the π-vector interaction can be found in a similar way:

$$\delta\varphi_{\rm vect} = \frac{1}{\gamma_1}\left(\frac{2\lambda_1}{L}\frac{N_3(2\omega)}{N_2^2(\omega)}\right)^{1/2}. \qquad (15)$$

One can see from expression (15) that the π-vector interaction is also noncritical with respect to the azimuthal angle. In addition, in contrast to (14), $\delta\varphi_{\rm vect}$ is independent of the azimuthal angle. The estimate made for the same values of parameters gives $\delta\varphi_{\rm vect} \approx 15^\circ$. Therefore, the spread angle of the azimuthal interaction for vector phase matching is greater than that for scalar phase matching.

4. Temperature tuning to phase matching in a $LiNbO_3$ crystal

Unlike Gaussian beams, Bessel beams possess a property of self-tuning to phase synchronism. The self-tuning can be realised by using the dependence of the wave detuning on the azimuthal angle between pairs of the interacting plane-wave BLB components, which was considered above. Therefore, the wave detuning can be compensated by changing the geometry of the vector interaction.

The self-tuning was earlier studied for the third harmonic generation in gas media [9]. In crystals, this effect can be observed upon SHG in the geometry when the BLB axis coincides with the direction of noncritical phase matching. In this case, it is necessary to change birefringence of a crystal by applying some external fields. Consider, for example, the temperature self-tuning in a uniaxial lithium niobate crystal when the BLB axis coincides with the direction of the 90° phase matching.

The conditions of the longitudinal and transverse phase matching for SHG have the form

$$n_{\rm o1}\cos\gamma_1 = n_2(\gamma_2)\cos\gamma_2,$$
$$n_{\rm o1}\sin\gamma_1\cos\varphi = n_2(\gamma_2)\sin\gamma_2. \qquad (16)$$

Taking into account that for small conicity angles γ_1 and γ_2, the refractive index for the extraordinary wave is $n_2(\gamma_2) = n_{\rm e2} + \delta\gamma_2^2\cos^2\varphi$, where $\delta = n_{\rm e2}^3(n_{\rm e2}^{-2} - n_{\rm o2}^{-2})/2$, equations (16) take the form

$$\cos^2\varphi = \frac{n_{\rm e2}^2 - n_{\rm o1}^2\cos^2\gamma_1}{n_{\rm o1}^2\sin^2\gamma_1},\ \cos\gamma_2 = \frac{n_{\rm o1}}{n_{\rm e2}}\cos\gamma_1. \qquad (17)$$

It follows from (17) that at the temperature T_1, when $n_{\rm e2}(T_1)/n_{\rm o1}(T_1) = \cos\gamma_1$, we have $\varphi = 90^\circ$, i.e., the π-vector phase matching is realised upon SHG. At the temperature T_2, when $n_{\rm e2}(T_2)/n_{\rm o1}(T_2) = 1$, we have $\varphi = 0$ and the collinear interaction is realised. Therefore, as the temperature varies in the range from T_1 to T_2, a variety of vector interactions is realised, i.e., the self-tuning to phase matching occurs.

The self-tuning to phase matching was experimentally realised for frequency doubling of a 1.064-μm Nd:YAG laser in a $LiNbO_3$ crystal of length 2 cm. A BLB at the fundamental frequency had the conicity angle in air equal to 2.5°. As the crystal temperature was varied, the interaction changed from the π-vector interaction at $t_1 \approx 60$ °C to the collinear interaction at $t_2 \approx 67$ °C. The second-harmonic field in the far-field zone at temperature t_2 represented an axial beam of the Gaussian type.

As the temperature was decreased, along with the axial beam a BLB was generated, which produced a circular intensity distribution in the far-field zone. The ring radius increased with decreasing temperature and became maximal at the temperature $t = t_1$. In this case, the intensity of the central maximum decreased to zero, whereas the total conversion efficiency during the temperature tuning remained approximately constant. In accordance with the calculation by formulas (17) using the Sellmeyer formulas [23], all types of the interactions, from collinear to π-vector, were realised within the temperature interval from 60 to 67 °C.

5. Transverse phase matching in SHG by Bessel beams

We assumed above by considering the longitudinal phase matching that the so-called transverse phase matching is simultaneously realised [20–22], when the mismatch of the transverse components of the wave vectors is zero. In the general case, there exists a finite transverse mismatch, which should be taken into account in the description of the interaction of BLBs. This is theoretically explained by the non-orthogonality of Bessel functions $J_0(q\rho)$ with different values of the parameter q at a finite interval.

The physical possibility of the interaction between BLBs when the transverse components of the wave vectors are not conserved is explained by the fact that these components are not coupled to the BLB momentum. Unlike the longitudinal phase matching, the transverse phase matching is independ-

ent of the crystal length and anisotropy and is determined only by the transverse size and the conicity angles of BLBs. The transverse phase matching is formally manifested in the dependence of the overlap integrals on the ratio of the conicity parameters of BLBs involved in the nonlinear process.

Fig. 4 shows the typical dependences of the overlap integral for SHG on the conicity parameter q_2 of the second harmonic for different numbers M_r of rings in the fundamental frequency BLB. One can see that the overlap integrals have two maxima whose location does not depend on the number of rings for large M_r ($M_r \geqslant 10$). One of the maxima corresponds to $q_2 \approx 2q_1$, and the second, to $q_2 \approx 0$. As M_r decreases, both these maxima approach each other and at $M_r = 1$ merge into one maximum at $q_2 \approx 1.2q_1$. This limiting case with one central maximum corresponds approximately to the interaction of Gaussian beams.

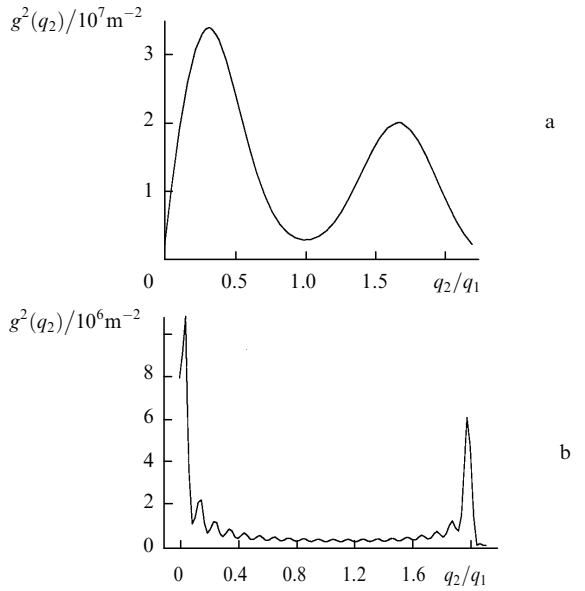

Figure 4. Dependences of the square of the overlap integral on the conicity parameter for the second harmonic for $R_B = 40$ (a) and 200 μm (b) and the number of rings $M_r = 2$ (a) and 20 (b).

By using plots of the overlap integrals versus the number of rings, we calculated the width δq_2 of the function $g^2(q_2, M_r)$ for different values of M_r. The width δq_2 proved to be virtually independent of M_r. The FWHM is described by the expression $\delta q_2 \approx \pi/R_B$ (where R_B is the BLB radius). This corresponds to the azimuthal angle

$$\delta\varphi_t(M_r) \approx M_r^{-1/2}. \tag{18}$$

Expression (18) is the azimuthal half-width of transverse phase matching, which is analogous to the half-width (14) of longitudinal phase matching introduced above. Let us compare the longitudinal ($\delta\varphi_{long}$) and transverse ($\delta\varphi_t$) mismatches for specific parameters of the SHG scheme. Fig. 5 shows the dependences $\delta\varphi_{long}$ and $\delta\varphi_t$ on the number of rings in the fundamental frequency BLB. We assume that $\Delta k_z(\varphi_0)$ in (14) is zero and take into account the relation $\gamma_1 \approx M_r\pi/R_B$ between the conicity angle and the number of BLB rings.

One can see that the number of possible channels of vector interactions for a small-diameter BLB under typical experimental conditions is restricted because of the longitudinal mismatch. As the diameter and the number of rings of the BLB are increased, the number of channels of vector interactions is restricted by the transverse mismatch. It is also important to note that the azimuthal width of phase matching for the BLB with a sufficiently great number of rings decreases and the inequality $\delta\varphi_t \ll \pi$ can be achieved. In this case, the regime of vector interactions approaches the azimuthally matched regime [20, 22].

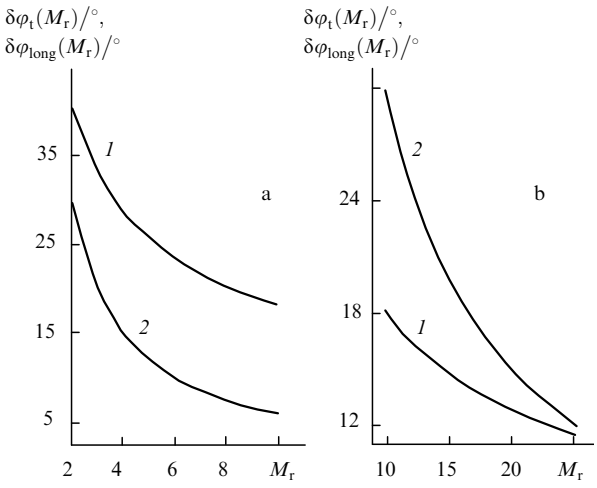

Figure 5. Dependences of the azimuthal phase matching width caused by the transverse ($\delta\varphi_t$) (*1*) and longitudinal ($\delta\varphi_{long}$) (*2*) detuning on the number of rings of the BLB at the fundamental frequency for $R_B = 40$ (a) and 200 μm (b). The crystal thickness $L = 5$ mm.

6. Theoretical model of three-wave mixing of BLBs

An increase in the role of vector interactions in nonlinear optics of BLBs is caused by the conical structure of their spatial frequency spectrum. It is important to note that the structure of the spatial spectrum in Bessel beams is optimal and is far simpler than that in Gaussian beams. This opens up new possibilities for the theoretical analysis of interactions of BLBs and for controlling the regime of their nonlinear interaction. In particular, an analytically solvable model of the three-wave mixing can be constructed, which will explain its basic features for low and medium conversion efficiencies. Consider this question in more detail for SHG of the oe–e type.

Let us represent the field strength at the fundamental frequency inside a crystal in the form

$$E_{1o,e}(\rho, z) = A_{1o,e}(z) j_0(q_1\rho) \exp(ik_{1oz,ez}z), \tag{19}$$

where $q_1 \approx k_0\gamma$; $k_{1oz,ez} \approx k_{1o,e} - q_1^2/2k_{1o,e}$, and

$$j_0(q_1\rho) = \frac{J_0(q_1\rho)}{\sqrt{\pi}R_B|J_1(q_1R_B)|} \text{ for } \rho < R_B,$$
$$j_0(q_1\rho) = 0 \text{ for } \rho \geqslant R_B \tag{20}$$

is the normalised Bessel function, so that the integral over the beam cross section is

$$2\pi\int_0^{R_B} j_0^2(q_1\rho)\rho\mathrm{d}\rho = 1.$$

Therefore, the fundamental radiation field in a nonlinear crystal is assumed to be localised within a cylindrical region of radius R_B. Hence, upon mixing of the BLBs at the fundamental frequency, the oe $\rightarrow$ e interaction results in the formation of the longitudinally homogeneous field at frequency 2ω with nonlinear polarisation and the transverse profile $\sim J_0^2(q_1\rho)$.

Expression (19) for the fundamental frequency field is valid if a change in its transverse structure during nonlinear conversion can be neglected. The conversion efficiency and the azimuthal width of phase matching caused both by the longitudinal and transverse mismatch play a decisive role in this case. If the azimuthal width of phase matching $\delta\varphi_0 \ll \pi$, the regime of azimuthally matched interactions is realised and distortions of the transverse structure of the BLBs are minimal even for the high conversion efficiency. In the case of a large azimuthal width (broadband interactions), a variety of vector interactions occur in the crystal, whose competition results in the distortion of the fundamental frequency field profile and in an increase in the efficiency of nonlinear process. Therefore, expression (19) is valid for azimuthally matched interactions and also for the interactions that are broadband over the azimuthal angle for low conversion efficiencies.

Let us represent the second-harmonic field amplitude as the Fourier – Bessel series

$$E_2(\rho, z) = \sum_{m=1}^{M} A_{2m} j_0(q_{2m}\rho) \exp(\mathrm{i}k_{2mz}z)\,, \tag{21}$$

where $q_{2m}R_B = (m - 0.25)\pi$ are zeroes of the Bessel function; $k_{2mz} \approx k_2 - q_{2m}^2/2k_2$. Therefore, expression (21) represents the expansion over the modes of a cylindrical region of radius R_B.

Using expressions (19) and (21), we obtain the following truncated equations for complex amplitudes A_{1o} and A_{1e} at the fundamental frequency and the second harmonic amplitude A_{2m}

$$\frac{\mathrm{d}A_{1o}}{\mathrm{d}z} = \mathrm{i}\sigma_{1o}A_{1e}^* \sum_{m=1}^{M} g_m A_{2m} \exp(\mathrm{i}\Delta k_{zm}z),$$

$$\frac{\mathrm{d}A_{1e}}{\mathrm{d}z} = \mathrm{i}\sigma_{1e}A_{1o}^* \sum_{m=1}^{M} g_m A_{2m} \exp(\mathrm{i}\Delta k_{zm}z), \tag{22}$$

$$\frac{\mathrm{d}A_2}{\mathrm{d}z} = \mathrm{i}\sigma_2 g_m A_{1o}A_{1e} \exp(-\mathrm{i}\Delta k_{zm}z),$$

where $\sigma_{1o,e} = 4\pi^2 d_{\mathrm{eff}}/\lambda n_{1o,e}$; $\sigma_2 = 8\pi^2 d_{\mathrm{eff}}/\lambda n_2$ are coefficients of nonlinear coupling; $n_{1o,e}$ and n_2 are the refractive indices at frequencies ω and 2ω; d_{eff} is the effective quadratic nonlinearity; and $\Delta k_{zm} = k_{2mz} - k_{1oz} - k_{1ez}$ are the wave detuning. The overlap integrals of the interacting fields are described by the expression

$$g_m = 2\pi \int_0^{R_B} j_0^2(q_1\rho) j_0(q_{2m}\rho)\rho \mathrm{d}\rho \quad (m = 1, 2, ..., M). \tag{23}$$

It follows from (22) that the introduction of the normalised Bessel functions allows one to describe the generation of harmonics and subharmonics by the same overlap integrals.

Equations (22) take into account the presence of phase mismatches, which depend on the mode number m. In the general form, this system can be investigated only numerically, which is of no interest. More interesting are the following particular cases, in which the specific features of BLBs are manifested:

(1) The interaction is azimuthally matched, so that only a single conversion channel m_0 can be taken into account. In this case, the overlap integral (23) has a sharp maximum at $m = m_0$, and only one term should be retained in the right-hand side of equations (22), which reduces these equations to the form used in the plane-wave approximation. It is known that the corresponding system can be solved exactly for an arbitrary conversion coefficient.

(2) The interaction is broadband over the azimuthal angle and the wave detuning Δk_{zm} are approximately the same. In this case, the system of equations (22) is solved in the specified intensity approximation [19]. Assuming $|A_{1o}|^2 = |A_{1e}|^2 = |A_1|^2/2$, we obtain the following equations for the partial amplitudes $a_{2m} = A_{2m}\exp(\mathrm{i}\Delta k_z z)$

$$\frac{\mathrm{d}^2 a_{2m}}{\mathrm{d}z^2} - \mathrm{i}\Delta k_z \frac{\mathrm{d}a_{2m}}{\mathrm{d}z} = -\sigma_1\sigma_2 g_m |A_1|^2 \sum_{s=1}^{M} g_s a_{2s}$$

$$(m = 1, 2, ..., M), \tag{24}$$

where $\sigma_{1o} = \sigma_{1e} = \sigma_1$.

By multiplying each of the equations (24) by g_m and summing their left- and right-hand sides, we obtain the following differential equation for the function $B(z) = \sum_{m=1}^{M} g_m a_{2m}$:

$$\frac{\mathrm{d}^2 B(z)}{\mathrm{d}z^2} - \mathrm{i}\Delta k_z \frac{\mathrm{d}B}{\mathrm{d}z} + K^2 B(z) = 0, \tag{25}$$

where the parameter K is determined by the sum over all generated modes of squares of the overlap integrals:

$$K = \left[\left(\frac{\Delta k_z}{2}\right)^2 + \sigma_1\sigma_2 |A_1|^2 \sum_{m=1}^{M} g_m^2\right]^{1/2}. \tag{26}$$

The solution of equation (25), taking into account the boundary conditions $A_{2m}(0) = 0$ has the form $B(z) = B_0 \sin(Kz)$. By substituting $B(z)$ into (24) and determining the constant B_0 from (22) we obtain

$$A_{2m} = \frac{4\pi\mathrm{i}\sigma_2 P_1 g_m \exp(-\mathrm{i}\Delta k_z z/2)}{cn_1 K} \sin(KL), \tag{27}$$

where L is the crystal thickness and $P_1 = cn_1|A_1|^2/8\pi$ is the fundamental frequency field power.

By using (27) and expression $P_2 = cn_2 \sum_m |A_{2m}|^2/8\pi$ the second harmonic power, we obtain the total SHG efficiency

$$\eta = \frac{P_2}{P_1} = \frac{P_1}{2P_0} \sum_{m=1}^{M} g_m^2 \frac{\sin^2(KL)}{K^2}, \tag{28}$$

where

$$K = \left[\left(\frac{\Delta k_z}{2}\right)^2 + \frac{P_1}{P_0}\sum_{m=1}^{M} g_m^2\right]^{1/2};$$

$$P_0 = \frac{cn_1^2 n_2 \lambda^2}{128\pi^5 d_{\mathrm{eff}}^2}$$

is the effective parameter having the dimensionality of power.

One can see from (28) that the SHG efficiency is substantially determined by the overlap integral g_m of the partial BLBs with the pump beam and by the total number M of the generated modes.

7. Experiment

7.1. SHG in Bessel beams

To study vector interactions of Bessel beams, experiments were performed on SHG in a KTP crystal in the oe $\rightarrow$ e interaction regime [19]. A crystal of thickness $L = 3$ mm was oriented in the XY plane at the angle $\varphi \approx 23^\circ$ to the X-axis in the direction of the type II collinear synchronism for Gaussian beams. A scheme of the experimental setup is shown in Fig. 6. Radiation from a 1.064-μm Nd:YAG laser passed through a diaphragm of diameter $D = 4$ mm and represented a super-Gaussian beam with a divergence of $\theta \leqslant 0.8$ mrad, a pulse duration of 5 ns, and an energy of 4 mJ.

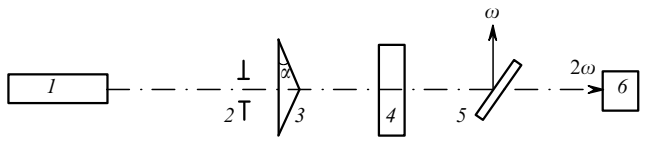

Figure 6. Scheme of the experimental setup: (*1*) Nd:YAG laser; (*2*) diaphragm; (*3*) axicon; (*4*) KTP crystal; (*5*) spectral beamsplitter; (*6*) power meter.

The spatial and energy characteristics of the second harmonic radiation were studied. It was found that the spatial profile of the second harmonic strongly depends on the orientation of the fundamental radiation BLB axis with respect to the phase matching direction. When the beam axis coincided with the phase matching direction, the intensity distribution of Gaussian beams was axially symmetric. The spatial structure of the radiation field in the far-field zone exhibited a central maximum and a concentric ring (Fig. 7), the ring radius being coincident with the radius of the ring for radiation at the fundamental frequency. Upon deviation of the BLB axis by the angle $\Delta\varphi$, the axial symmetry of the second harmonic field was destroyed; and when the value of $\Delta\varphi$ was sufficiently large, SHG was observed only in the axial beam.

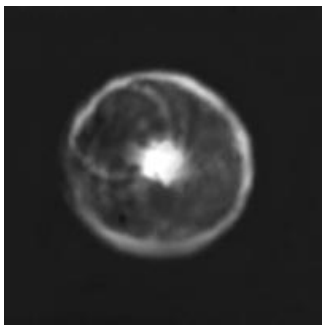

Figure 7. Spatial structure of the second-harmonic field in the far-field zone upon mixing of two Bessel beams.

The measurements of the divergence of the axial beam revealed its dependence on the longitudinal coordinate. In the central zone, i.e., for 6 cm $< z <$ 10 cm, the divergence was approximately 1.7 mrad. Near the axicon and also near the BLB focus, the divergence increased up to 2.5–3 mrad.

The energy parameters of the second harmonic radiation were measured for a super-Gaussian beam at the fundamental frequency with a fluence of 25 MW cm^{-2}. The total conversion efficiency nonmonotonically depends on the longitudinal coordinate and its maximum value is $\sim 21\%$ (Fig. 8). The efficiency of conversion to the axial beam similarly depends on the longitudinal coordinate. In the absence of an axicon, the conversion efficiency for a super-Gaussian beam was $\sim 7\%$ for the same intensity of the fundamental radiation. Note that a relatively low conversion intensity for a super-Gaussian beam is explained by the fact that its focusing to a crystal is not optimal.

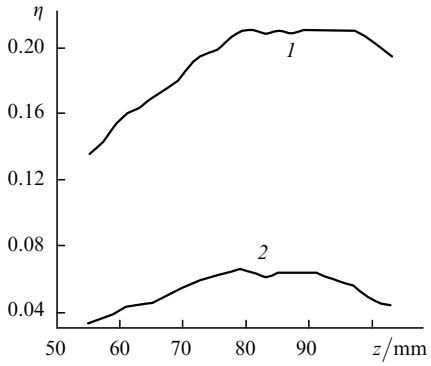

Figure 8. Dependences of the total SHG efficiency (*1*) and the efficiency of conversion to the axial beam (*2*) on the distance from an axicon.

The experimental results well agree with the above theoretical model of SHG and with the calculations of longitudinal and transverse phase matching for BLBs. As follows from sections 2 and 5, the channels of vector interactions can be limited both by the longitudinal and transverse mismatch of the fields.

In the experiment discussed, a super-Gaussian beam was converted to a BLB using an axicon made of a glass with the refractive index $n = 1.5$. The angle at the axicon base was $\alpha = 2^\circ$. Therefore, the conicity angle of the BLBs being formed was equal to 1°, whereas the angular width of the longitudinal phase matching for the oe $\rightarrow$ e interaction in a KTP crystal was $\sim 2^\circ$. Thus, the possible vector interactions in the crystal were mainly restricted by the transverse phase matching conditions.

To specify these conditions, note that a BLB was formed behind the axicon in the interval $0 < z < z_f$, where $z_f = 2R_B/\gamma$ is the focal length of the BLB of radius R_B. In experiments, the focal length of both BLBs at the fundamental frequency was ~ 12 cm. The radius of the beams at the distance equal to a half the focal length was approximately 1 mm and the number of rings in the beam was $M_r = 33$. The overlap integral for these parameters of the beams has a characteristic form (Fig. 4b) with two narrow maxima located at $q_2 \approx 2q_1$ and $q_2 \approx 0$.

By comparing these values of q_2 with the conicity parameters $q_{2m} = 2q_1 \cos(\varphi_m/2)$ (where φ_m is the azimuthal angle

between the transverse projections of the wave vectors of BLBs), we found that the circular field and the axial beam observed in the experiment are caused by π-vector and collinear interactions, respectively. In reality, along with these interactions, the interactions adjacent to them (within the width of the maxima of the overlap integral) are also realised.

Thus, the spatial structure of the second-harmonic field is determined by the dependence of the overlap integrals on the mode index m or the conicity parameter q_{2m} of the BLB at the double frequency, which depends on the mode parameter. It follows from expression (18) that the azimuthal width of phase matching is $\delta\varphi_t \approx 10^\circ$. Therefore, a few ($\sim 2-4$) second harmonic modes can be generated within each maximum of the overlap integrals.

The SHG efficiency can be calculated from expression (28). For the KTP crystal cut under study, $d_{\text{eff}} = d_{15}\sin^2\varphi_{\text{pm}} + d_{24}\cos^2\varphi_{\text{pm}}$ and, according to [23], $d_{15} = 1.9$ pm V^{-1} and $d_{24} = 3.4$ pm V^{-1}. By substituting the values of n_1 and n_2 from [23] and the fundamental harmonic BLB parameters $P_1 = 8\times10^5$ W and $R_B = 1$ mm into (28), we obtain $\eta \approx 0.19$, in good agreement with the experimental value $\eta_{\text{exp}} \approx 0.21$.

Using expressions (27) for the partial amplitudes A_{2m}, we can calculate the transverse profile $E_2(\rho)$ of the second-harmonic field:

$$E_2(\rho) \sim \sum_m A_{2m} j_0(q_{2m}\rho). \tag{29}$$

The transverse distribution of the second-harmonic intensity at the crystal output, which was calculated by formula (29), represents the interference structure with a narrow central maximum and a few weak side maxima [19]. This spatial structure of the field is also established inside the crystal at a small distance from its input face.

Therefore, upon SHG in partial Bessel beams, the interference spatial redistribution of the second-harmonic intensity takes place. Namely, a predominantly destructive interference is realised at the beam periphery, whereas at the beam centre, the constructive interference occurs.

In other words, the second-harmonic intensity is transferred efficiently from the beam periphery to its centre. It is interesting that a similar result can be obtained by assuming that SHG takes place predominantly at the central part of the BLB, where the field intensity is maximal. In this case, the depletion of the field energy at the beam centre can be compensated by its supply from the BLP periphery, similarly to the known linear effect of the reconstruction of the transverse profile of a BLB behind an opaque screen.

7.2. SHG upon mixing of Bessel and Gaussian light beams

Along with SHG by purely Bessel beams, of interest is the study of the interaction between Bessel and Gaussian beams. To elucidate the properties of such interaction, we studied SHG for a neodymium laser in a KTP crystal of thickness 3 mm. A comparative analysis of SHG of the type II was performed for three variants (channels) of mixing of the fundamental frequency beams: (1) two Bessel beams, (2) Bessel beam and Gaussian beam, and (3) the general case of the interaction of Bessel and Gaussian beams of both polarisations.

Because the crystal thickness was small, the longitudinal phase matching took place both for collinear and vector interactions. The BLB pulse energy $W_B \approx 10.8$ mJ was fixed, whereas the Gaussian beam pulse energy W_G was varied between ~ 2.6 and 27 mJ. The study of the dependence of the conversion efficiency $\eta_{2\omega}$ on the total radiation energy at the fundamental frequency showed that the SHG efficiency for the $o_1^G + e_1^G \rightarrow e_2^G$ interaction proved to be higher than for the mixing of Gaussian and Bessel beams. At the same time, for the $o_1^B + e_1^B \rightarrow e_2^B$ interaction for the above-mentioned energy of BLBs, the SHG efficiency $\eta_{2\omega}^B \approx 12\,\%$, which is higher than the conversion efficiency $\eta_{2\omega}^G \approx 9$ for the Gaussian beam of the same energy.

Fig. 9 shows the transverse intensity distribution in the far-field zone for the second interaction channel. The single-ring structure of the second-harmonic field suggests that the noncollinear phase matching takes place upon SHG. The phase matching of this type is realised upon the interaction of the plane-wave components of a Gaussian beam, which are localised near its axis, with all Fourier components of a cone of the wave vectors of the BLBs. Comparison of Figs 9 and 7 shows that the radius of the circular field for the second interaction channel is two times smaller than that for the first channel. This means that the conicity angle of the second-harmonic radiation upon mixing of Bessel and Gaussian beams is two times smaller than the conicity angle of the BLB at the fundamental frequency. This result completely agrees with the calculation of the transverse phase matching condition for the interaction channels under study.

Figure 9. Far-field spatial structure of the second harmonic generated upon mixing of Bessel and Gaussian beams.

Fig. 10 shows the dependence of the integral of overlap of Bessel and Gaussian beams on the ratio q_2/q_1 of the conicity parameters. The calculation was performed in accordance with experimental conditions for a BLB of radius 1.7 mm and the conicity angle of 0.2° and a Gaussian beam of radius 1.2 mm. The study showed that the maximum overlap integral is realised for the second-harmonic BLB of radius ~ 1 mm. One can see from Fig. 10 that the transverse spatial matching is realised at $q_2 = q_1$.

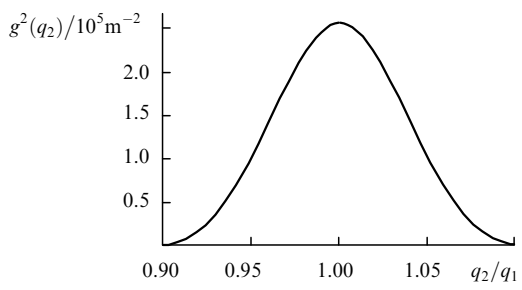

Figure 10. Square of the overlap integral of Bessel and Gaussian beams as a function of the conicity parameter of the second-harmonic BLB.

Note also that the angular width of the transverse matching for the interaction in the second channel is greater than in the first channel. This results in an increase in the width of the circular field in the far-field zone upon mixing of Bessel and Gaussian beams. As the radius of the Gaussian beam decreases, the number M_r of rings of the BLB that overlap with the Gaussian beam also decreases. In this case, the structure of the overlap integral is conserved down to $M_r = 2$, however, the width of the maximum increases. This results in the increase in the width of the second-harmonic circular field. In the limiting case of the overlap of the Gaussian beam with one central maximum of the BLB, the circular structure of the second-harmonic field disappears and the generation of the axial beam of the Gaussian type takes place.

Therefore, to produce vector interactions upon SHG by Bessel and Gaussian beams, the longitudinal and transverse phase matching should simultaneously take place. This conclusion is followed from the above theoretical treatment and is confirmed experimentally.

We also studied the general case of SHG by exciting Bessel and Gaussian beams of both polarisations in a crystal. The transverse distribution of the second-harmonic intensity represented in the general case two rings, which corresponded to two types of transverse phase matching for the $o_1^G + e_1^B \to e_2^B$, $o_1^B + e_1^G \to e_2^B$ and $o_1^B + e_1^B \to e_2^B$ interactions, and a central maximum related to the $o_1^G + e_1^G \to e_2^G$ and $o_1^B + e_1^B \to e_2^G$ processes. An interesting feature of this SHG regime is the possibility of the interference of nonlinear processes for the $o_1^G + e_1^B \to e_2^B$ and $o_1^B + e_1^G \to e_2^B$ interactions. In particular, we observed the interference quenching of the second-harmonic radiation when the directions of polarisation of the beams made an angle 45° with the XY plane of the KTP crystal.

8. Generation of the sum frequency by Bessel light beams

The sum frequency generation (SFG) by Bessel beams was observed in an Y-cut KTP crystal [26]. The sum frequency was generated due to the oe–o interaction upon the addition of a BLB from a Nd:YAG laser ($\lambda_1 = 1064$ nm) polarised along the X-axis and a BLB from a Ti:sapphire laser ($\lambda_2 = 808 - 830$ nm) polarised along the Z-axis. Upon mixing of the two BLBs, the generation of blue emission at the sum frequency polarised along the X-axis was observed.

A scheme of the experimental setup is similar to that shown in Fig. 6. An acousto-optically Q-switched Nd:YaG laser emitted 120-ns light pulses simultaneously at $\lambda_1 =$ 1064 nm and at the second harmonic. The output power was 100 mW at both wavelengths and the pulse repetition rate was 1–3 kHz.

The green emission from a neodymium laser was used to pump a Ti:sapphire laser, which emitted 5-mW pulses tunable in the wavelength region $\lambda_2 = 808 - 830$ nm. Gaussian beams at frequencies ω_1 and ω_2 were focused with a spherical lens in such a way that their diameters in the input plane of an axicon were approximately 200 μm.

The axicon with the refractive index $n = 1.5$ and the angle at the base $\alpha = 5°$ transformed Gaussian beams to Bessel beams. A KTP crystal of size $3 \times 3 \times 5$ mm was placed at a distance of 0.5 mm from the axicon. When the axicon was absent, the sum frequency was generated in an Y-cut KTP crystal under the conditions noncritical phase matching for the wavelengths 1064 and 808 nm [27]. The dependence of the conversion efficiency on the wavelength λ_2 is compared in Fig. 11 with the efficiency of SFG by Gaussian beams (in the absence of the axicon).

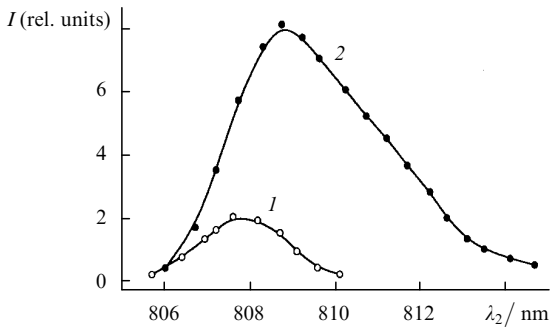

Figure 11. Dependences of the sum frequency intensity on the wavelength of a Ti:sapphire laser upon mixing of Gaussian (*1*) and Bessel (*2*) beams.

The spatial structure of the beams was analysed in the focal plane of the lens using a CCD camera placed 60 mm behind the axicon. Figs 12 a–c show the Fourier spectra of the BLB from a Nd:YaG laser and Ti:sapphire laser, and of the emission at the sum frequency, respectively. The circular intensity distribution suggests that the beams have the Bessel structure, a small ellipticity being caused by the anisotropy of a KTP crystal in the XZ plane. It should be emphasised that the radius of the emission ring at the frequency ω_3 coincides with radii of rings at frequencies ω_1 and ω_2. By tuning the wavelength of a Ti:sapphire laser, we obtained the maximum SFG efficiency at $\lambda_2 = 808.5$ nm.

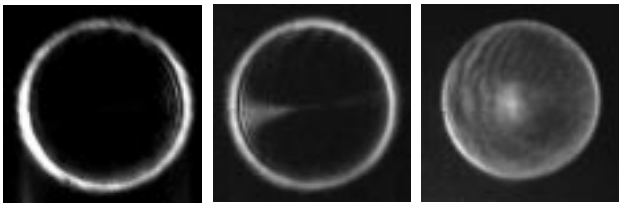

Figure 12. Spatial Fourier spectra of light beams at the wavelengths 1064 (a) and 808.5 nm (b) and of the sum frequency radiation (c).

The theoretical description of SFG can be conveniently performed by representing the sum frequency field as a superposition of the fields of mode Bessel beams. Then, the field strengths of two BLBs with frequencies ω_1 and ω_2 propagating along the Y-axis and polarised along the X- and Z-axes have the form [see also (19)]

$$E_{1,2}(\rho, y) = A_{1,2}(y) j_0(q_{1,2}\rho) \exp(\mathrm{i}k_{1,2y}y). \tag{30}$$

The mixing of differently polarised BLBs due to the type II oe–o interaction in a crystal results in the formation of a cylindrically symmetric field of nonlinear polarisation at the frequency ω_3 with the radius R_B equal to the radii of BLBs at frequencies ω_1 and ω_2.

Let us represent the sum frequency field $E_3(\rho, y)$ as the expansion in the modes of the cylindrical region of radius R_B:

$$E_3(\rho, y) = \sum_{m=1}^{M} A_{3m}(y) j_0(q_{3m}\rho) \exp(\mathrm{i}k_{3my}y), \tag{31}$$

where $q_{3m} = (m - 0.25)\pi/R_B$. By using (30) and (31), we can obtain the truncated equations for complex amplitudes

A_1, A_2, and A_{3m}, which are similar to (22), with the overlap integral

$$g_m = 2\pi \int_0^{R_B} j_0(q_1\rho) j_0(q_2\rho) j_0(q_{3m}\rho)\rho \mathrm{d}\rho. \quad (32)$$

The conversion efficiency $\eta_3 = P_3/(P_1P_2)^{1/2}$ (where $P_{1,2}$ is the power of the interacting waves), in the specified intensity approximation and for the same wave detunings $\Delta k_{my} = \Delta k_y$, is described by the expression

$$\eta_3 = \frac{(P_1P_2)^{1/2}}{P_0} \sum_{m=1}^{M} g_m^2 \frac{\sin^2(KL)}{K^2}, \quad (33)$$

where

$$K = \left[\left(\frac{\Delta k_y}{2} \right)^2 + \left(\frac{\lambda_3 P_1}{\lambda_2 P_0} + \frac{\lambda_3 P_2}{\lambda_1 P_0} \right) \sum_{m=1}^{M} g_m^2 \right]^{1/2}.$$

As in the case of SHG, the sum frequency radiation is generated in the general case simultaneously in many channels. However, the actual efficiency of conversion to different channels is different because the corresponding overlap integrals and wave detunings are different. We calculated the overlap integrals by formula (32) using not rigorous mathematical Bessel functions but the amplitude-phase distributions of the fields at the fundamental frequencies behind the axicon, which were preliminary calculated with the scheme parameters corresponding to the given experiment.

Fig. 13 shows typical field intensity distributions at two distances from the axicon. One can see that because of the sharp focusing of the field, the Bessel beams contain a small number of rings. Fig. 14 shows the dependences of the squares of overlap integrals for the wavelengths $\lambda_1 = 1064$ nm and $\lambda_2 = 808.5$ nm on the mode index of the sum frequency BLB. In both these cases, the overlap integrals have two maxima. The width of the maxima is approximately equal to three mode indices lying in the regions $m = 3-5$ and $20-22$. Therefore, two groups of the modes with these mode indices make the dominant contribution to the SFG.

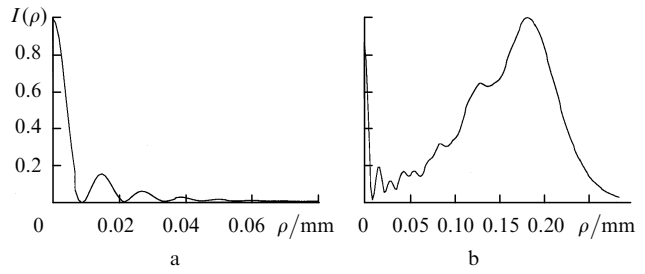

Figure 13. Distributions of the field intensity 1 (a) and 6 mm (b) behind an axicon.

To determine the physical nature of the maxima, we consider the phase matching conditions for transverse components of the wave vectors (see also Fig. 1b)

$$q_1 \cos(\Delta\varphi_1) + q_2 \cos(\Delta\varphi_2) = q_{3m},$$
$$q_1 \sin(\Delta\varphi_1) - q_2 \sin(\Delta\varphi_2) = 0. \quad (34)$$

If the azimuthal angles $\Delta\varphi_{1,2} \approx 0$, then we find from (34) that $m_{\mathrm{coll}} \approx (q_1 + q_2)R_B/\pi$, while for $\Delta\varphi_1 + \Delta\varphi_2 \approx \pi$, we

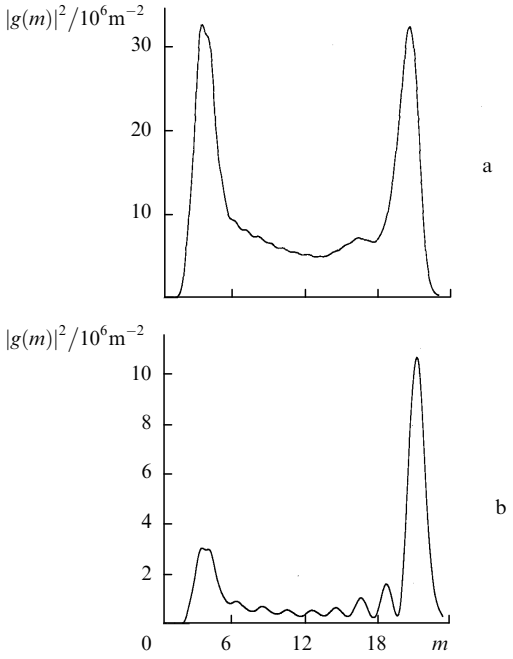

Figure 14. Dependences of the square of modulus of the overlap integral on the mode conicity index of the BLB at the sum frequency for distances 2 (a) and 3.5 mm (b) from an axicon with $R_B = 90$ μm, $\gamma = 2.5°$, $\lambda_1 = 1.06$, μm, $\lambda_2 = 0.8085$ μm.

have $m_{\mathrm{vect}} \approx (q_1 - q_2)R_B/\pi$. By substituting parameters $q_{1,2}$ and R_B into these formulas, we obtain that $m_{\mathrm{coll}} \approx 21$ and $m_{\mathrm{vect}} \approx 3$, in good agreement with the position of the maxima of overlap integrals (Fig. 14). This means that the first group of sum frequency modes is generated due to the interactions that are close to the π-vector interactions, while the second group of modes is generated due to almost collinear interactions. The behaviour of the overlap integrals described above is virtually the same over the entire range of the wavelengths λ_2.

The efficient SFG is possible only when both the transverse and longitudinal phase matching take place. If the longitudinal phase matching is satisfied for both groups of modes, then the radiation at the fixed sum frequency will represent two BLBs with different conicity angles. In this case, the intensity distribution in the far-field zone will represent two rings. The ring of a larger diameter is caused by collinear interactions, while the ring of a smaller diameter is caused by π-vector interactions.

Using the Sellmeyer equations for a KTP crystal, we can show that, for the axicon with the angle equal to 5°, the longitudinal wave detuning for collinear interactions vanishes at $\lambda_2 = 809$ nm. This result exactly corresponds to the generation of a circular beam due to collinear interactions, which was observed in the experiment (Fig. 12). In this case, the conicity angle of the beam coincides with the conicity angles of BLBs at fundamental frequencies. A small width of the circular field of the Fourier spectrum means that the sum frequency radiation can be sufficiently accurately approximated by a single-mode BLB.

The wavelength of the longitudinal phase matching for π-vector interactions proves to be equal to 825 nm. However, unlike collinear interactions, vector interactions have not been observed in our experiments. To understand the reason for the absence of the second ring, we studied the structures of the field and the overlap integral behind the axicon

(Fig. 14). One can see from the comparision Figs 14a and 14b that the maximum of the overlap integral corresponding to the π-vector interaction decreases upon moving away from the axicon.

In addition, at the distance $z > z_f/2$, from the axicon (where $z_f \approx 3$ mm), the region occupied by the BLB decreases, whereas the region occupied by a diverging conical beam correspondingly increases. Note that collinear interactions continue within the conical beam, whereas π-vector interactions cannot occur. For this reason, vector interactions are suppressed in our experiments. It follows from the above discussion that the contribution from vector interactions will increase with increasing focal length of the BLB. This is achieved by decreasing the refraction angle of the axicon and also by decreasing the degree of focusing of the incident beams.

The conical structure of the spatial frequency spectrum of BLBs facilitates their application for conversion of multifrequency laser radiation. For this purpose, the relation between the wavelength of the longitudinal phase matching and the conicity angle is used. In the case of collinear phase matching, this relation has the form

$$\sin^2\gamma = [N_y^{-2}(\lambda_2) - N_z^{-2}(\lambda_2)]^{-1}$$

$$\times\left\{\lambda_1^2\lambda_3^2[\lambda_1\lambda_2 N_x(\lambda_3) - \lambda_2\lambda_3 N_x(\lambda_1)]^{-2} - N_z^{-2}(\lambda_2)\right\} \quad (35)$$

and is plotted in Fig. 15. One can see that the wavelength of collinear phase matching monotonically increases with increasing conicity angle of the BLB. Because the conicity angle can be changed using a simple optical scheme, this method for generating the tunable sum frequency radiation is of practical interest.

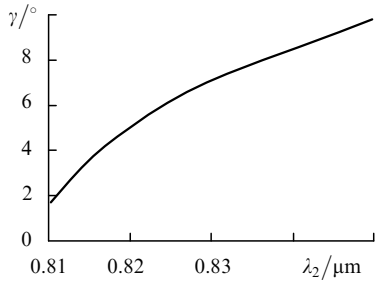

Figure 15. Dependence of the BLB conicity angle corresponding to the collinear phase matching on the wavelength of a Ti:sapphire laser.

The SFG can be also obtained by mixing the beams with a spatial Fourier spectrum consisting of several cones (N-cone BLBs). The N-cone BLBs can be produced by using a simple scheme consisting of several axicons in series with different apex angles. One of the axicons should have a relatively large angle α_0, while the other axicons should have small angles $\Delta\alpha$, $2\Delta\alpha, \ldots, N\Delta\alpha$. The axicons are separated by half focus lengths. One can easily verify that each subsequent axicon will double the number of cones of the spatial frequency spectrum of the field produced by a preceding axicon. Therefore, the output field will be a 2^N-cone BLB.

Let us illustrate the application of the multicone BLB for the case when one of the fields is quasi-monochromatic at the frequency ω_1, while the other field is multimode with frequencies lying in the interval $\omega_2' - \omega_2''$. We assume that BLBs at these frequencies are formed in such a way that the quasi-monochromatic beam is multicone, whereas the broadband beam is single-cone. As the conicity angle of one of the beams changes, the frequency at which the longitudinal phase matching is realised also changes. This means that each of the N BLBs at the frequency ω_1 will interact with the multimode BLB within some spectral range $\Delta\omega$, which is determined by the widths of the longitudinal and transverse phase matching.

As a whole, a set of N beams will cover the spectral range of width $\sim N\Delta\omega$. This method will be efficient if the spectrum of one of the fields is discrete and the number N is relatively small, because the splitting of the initial beam results in the N-fold decrease in the power of partial BLBs at the frequency ω_1. This means that the method of splitting of the broadband beam into N Bessel beams with different frequencies is more efficient than the method of splitting of quasi-monochromatic beam. However, this method requires the use of a comparatively complex device of the axicon type with the wavelength-dependent refraction angle.

Note that we have observed this effect in the experiments on mixing of the beams from a neodymium laser and a Ti:sapphire laser when the input face of a KTP crystal was located near the axicon focus [26]. In this case, the transverse dimensions of the overlap of the fields are small, and Bessel beams contain 2–3 rings. The Fourier spectrum of such beams exhibits additional rings and a central maximum, i.e., the beams can be classified as multicone beams. Correspondingly, the sum frequency field was also multicone, with the frequency shift on passing from one cone to another.

9. Azimuthally correlated BLBs

We studied above theoretically and experimentally the SHG and SFG by Bessel beams. The main attention was paid to the properties of nonlinear conversion caused by various vector interactions that are specific for BLBs. Another very important problem concerning the nonlinear optics of BLBs is the efficiency of nonlinear frequency conversion of these beams and its comparison with the frequency conversion efficiency for Gaussian beams.

It seems that the study of this problem using conventional approaches, i.e., without the nontrivial use of the BLB specific properties, will not allow one find the regimes of nonlinear frequency conversion of BLBs whose efficiency would be higher than that for the Gaussian beams. The exception is the case of small conversion efficiencies (the linear SHG regime) for which it was established that the use of BLBs provides the efficiency that is 50% higher compared to Gaussian beams [8, 29].

To analyse the general case of an arbitrary SHG efficiency, we compare the overlap integrals for beams of both types. We will describe the Gaussian field strength by the normalised function

$$E_G(\rho, w) \sim \frac{\exp(-\rho^2/2w^2)}{\sqrt{\pi}w}.$$

Then, the overlap integral for the SHG has the form

$$g_G(w_2) = \frac{2w_2}{w_1^2 + 2w_2^2}.$$

For $w_2 = w_1/\sqrt{2}$, the function $g_G(w_2)$ takes the maximum value equal to $1/\sqrt{2}w_1$. For the beam of radius 50 μm, we obtain $g_G \approx 1.4 \times 10^4$ m^{-1}. To obtain the maximum

value of the overlap integral in the case of BLBs, one should use the beams with a small number of rings. In this case, the minimum number of the BLB rings at which the Fourier spectrum retains its circular structure is equal to two. In this case, it is possible to obtain the value of $g_B \sim (0.3 - 0.4)g_G$ by choosing the appropriate radius of the beam.

Therefore, the optimal focusing of Gaussian beams allows one to obtain the greater value of the overlap integral compared to that obtained upon focusing of BLBs. In this sense, the nonlinear optical efficiency of Gaussian beams is higher than that of BLBs, which is also confirmed by the numerical calculations performed in Ref. [29]. Comparison of the SHG efficiencies based on the analysis of the overlap integrals is correct when these integrals do not change because of nonlinear amplitude-phase distortions of the transverse profiles of the beams.

There is reason to assume that BLBs are the most stable namely to nonlinear distortions. This is explained by the nonlocality of frequency conversion of BLBs, which is manifested in the dependence of the nonlinear optical process on the spatial Fourier components of the BLB rather than on the local intensities, as in the case of Gaussian beams. In this case, the predominantly nonlocal SHG of Bessel beams will occur with decreasing azimuthal width of the phase matching.

As follows from the results presented in previous sections, in the case of the BLB, the azimuthal width can be obtained at which the fields generated within a crystal are single-mode. The single-mode condition is more easily satisfied in various intracavity schemes. The generation of single-mode BLBs in connection with the parametric frequency conversion was discussed in Ref. [22] and was called azimuthally matched. Below, we will show that the beam overlap integrals considerably increase due to the establishment of the azimuthally matched interaction.

Let us consider, for example, the SHG and study the factor ρ in the nonlinear polarisation at the double frequency, which depends on the transverse coordinate,

$$p_2(\rho) = J_0^2(q_1\rho). \tag{36}$$

Let us transform (36), by introducing the function in the cylindrical coordinate system, which is analogous to a plane wave in the Cartesian system

$$\psi_1(\rho, \varphi) = \exp(\mathrm{i}q_1\rho\cos\varphi). \tag{37}$$

This function is the azimuthal or angular spectral component of the BLB, because the angular superposition of the functions (37) within the range $0 - 2\pi$ is the BLB amplitude

$$J_0(q_1\rho) = \frac{1}{2\pi}\int_0^{2\pi} \psi_1(\rho, \varphi)\mathrm{d}\varphi. \tag{38}$$

By using the azimuthal spectral components (37), we rewrite (36) in the form

$$p_2(\rho) = \frac{1}{2\pi}\int_0^{2\pi} p_2(\rho, \varphi)\mathrm{d}\varphi, \tag{39}$$

where

$$p_2(\rho, \varphi) = \frac{1}{\pi}\int_0^{\pi} \psi_1(\rho, \varphi - \Delta\varphi)\psi_1(\rho, \varphi + \Delta\varphi)\mathrm{d}(\Delta\varphi). \tag{40}$$

The structural feature of the function $p_2(\rho)$ is that it can be treated as a result of two successive averagings. At first, the product of the spectral components $\psi_1(\rho, \varphi - \Delta\varphi)\psi_1(\rho, \varphi + \Delta\varphi)$ is averaged over the azimuthal angle $\Delta\varphi$ [formula (40)] and then the result is averaged over the angle φ [formula (39)]. Note here that the absence of a weight function depending on $\Delta\varphi$ in the integrand in (40) could be treated as a consequence of the equal probability of the mutual orientation of the azimuthal components at the fundamental frequency. However, as was shown above, the angle $\Delta\varphi$ between the plane-wave components of the BLB at the fundamental frequency is not arbitrary in the process of generation of a subharmonic under the conditions of selection of the types of vector interactions. This angle is determined by the phase matching conditions, and in the case of collinear phase matching under study, is close to zero.

Therefore, the equilibrium mutual orientation of the azimuthal components of BLBs at frequencies 2ω and ω is established because there is no selection of the vector interactions. And vice versa, the selection of vector interactions produces the nonequilibrium mutual orientation of the azimuthal components of BLBs. In the latter case, the formation of nonlinear polarisation can be correctly described by introducing the corresponding weight function $\mu_{11}(\Delta\varphi)$ into (40):

$$p_2(\rho, \varphi) = \int_0^{\pi} \mu_{11}(\Delta\varphi)\psi_1(\rho, \varphi - \Delta\varphi)\psi_1(\rho, \varphi + \Delta\varphi)\mathrm{d}(\Delta\varphi). \tag{41}$$

The function $\mu_{11}(\Delta\varphi)$ represents the probability density for the mutual orientations of the plane-wave components of the BLB at the fundamental frequency, which differ by the angle $\Delta\varphi$. In a particular case of the nonselective interaction, one should set $\mu_{11} = 1/\pi$ [formula (41)].

The introduction of the probability density function is equivalent to the assumption that at the stage of vector interactions upon SHG, there appears the autocorrelation of the azimuthal orientation of the plane-wave components of BLBs at the frequency ω within some range of angles $\delta\varphi$. As $\delta\varphi$ decreases, the probability density function $\mu_{11}(\Delta\varphi)$ narrows down. The limiting case $\delta\varphi \to 0$ corresponds to the azimuthally matched interaction. This limiting regime can be described mathematically by assuming that

$$\mu_{11}(\Delta\varphi) = \delta(\Delta\varphi), \tag{42}$$

where $\delta(x)$ is the delta function. By substituting (41) into (42) and integrating, we obtain

$$p_2(\rho, \varphi) = \psi_1(\rho, \varphi)\psi_1(\rho, \varphi). \tag{43}$$

Expression (43) corresponds to some pure state in which the average value represents a product of the spectral components. By substituting (43) into (39) and integrating, we obtain

$$p_2(\rho) \sim J_0(2q_1\rho). \tag{44}$$

Therefore, the nonlinear polarisation at the double frequency for the azimuthally matched BLB at the fundamental frequency is proportional to the first power of the Bessel function rather than to the product of two Bessel functions. Because the spatial profiles of the nonlinear polarisation and the second harmonic field coincide, the overlap integral (23)

will be maximal: $g_2 = \sqrt{W_2}/W_1$, where

$$W_{1,2} = \pi R_B^2 [J_0^2(q_{1,2}R_B) + J_1^2(q_{1,2}R_B)].$$

As was shown in Ref. [28], where the mutual azimuthal matching of the BLBs at the fundamental and double frequency was considered, the overlap integral for the subharmonic generation is $g_1 = 1/\sqrt{W_2}$. The product of the overlap integrals, which determines the total SHG efficiency, is $g_1 g_2 = g_B^2 = 1/W_1$. It was shown above that a similar parameter for Gaussian beams is $g_G^2 = 1/2w_1^2$. The ratio of the squares of the overlap integrals, taking into account the explicit expression for the power integral W_1 is

$$\frac{g_B^2}{g_G^2} = \frac{2w_1^2}{\pi R_B^2 [J_0^2(q_1 R_B) + J_1^2(q_1 R_B)]}. \quad (45)$$

Let us find the ratio (45) in the case of equal diffraction lengths $Z_{G,B}$ of the Gaussian and BLB beams. Assuming that $Z_G = 2kw_1^2$ and $Z_B = 2R_B/\gamma$ and using asymptotic approximations for Bessel functions, we find from (45), virtually without loss of generality, that $g_B^2/g_G^2 \approx 1$. Therefore, the effective overlap integrals for the azimuthally matched BLBs are equal to maximum overlap integrals for Gaussian beams. In this case, because of the coincidence of the spatial structures of the nonlinear polarisation and the generated field, one should expect that nonlinear distortions in the case of BLBs will be substantially weaker than for Gaussian beams.

10. Conclusions

The study of the frequency conversion of laser radiation in Bessel light beams showed that the specific features of the application of BLBs compared to Gaussian beams are related to the fundamental difference between the spatial frequency spectra of these beams. Because of the conical structure of the spatial spectrum of BLBs, it is possible to realise and control various vector interactions in them.

We have found the limitations imposed by the longitudinal wave detuning on the azimuthal symmetry of nonlinear optical processes in the general case of biaxial crystals under the conditions of critical and noncritical phase matching. We have studied the transverse phase matching, which are manifested in the dependence of the overlap integrals on the parameters of interacting BLBs. The role of the longitudinal and transverse phase matching has been studied in detail for the SHG in a Nd:YAG laser and SFG for Nd:YAG and Ti:sapphire lasers.

It is shown that the advantage of BLBs is the possibility of generation of tunable radiation at the sum frequency. The wavelength tuning is performed by varying the conicity of the fundamental frequency beam. The possibility is shown of the efficient generation of the second-harmonic BLB tunable over the conicity angle due to the self-tuning of vector interactions to the longitudinal phase matching. This effect was experimentally observed for the SHG in lithium niobate with the temperature-tunable phase matching angle.

The azimuthal phase matching width caused by the longitudinal and transverse wave detunings is calculated. The regime of azimuthally matched interactions is separated, which is realised in the case of a small azimuthal phase matching width when the generated beams are approximately single-mode BLBs. It is predicted that the establishment of azimuthally matched interactions results in the appearance of matching between the azimuthal components of the beams. The overlap integral for the azimuthally matched beams is greatly increased and their spatial structure is not destroyed upon their interaction.

The BLBs are promising for cascade frequency doubling and mixing for obtaining the UV radiation. Upon tuning to the π-vector phase matching, the second-harmonic radiation represents an axial beam, while radiation at the fundamental frequency represents a circular beam. As a result, these beams are spatially separated and there is no need in the frequency-selective elements, whose fabrication for the UV region involves significant technological difficulties.

Of interest is the study of the nonlinear frequency conversion of BLBs with the wave front dislocations. The BLB frequency doubling and summation permits the controllable generation and destruction of dislocations [30], which shows promise for realisation of logical and arithmetical operations. The higher-order BLBs can be obtained by the recent method [31] using biaxial crystals, which also can be applied for the transformation of the Bessel function order.

Acknowledgements. The authors thank A G Mashchenko for placing the experimental data on the study of the temperature-tuned SHG in lithium niobate at our disposal. This work was partially supported by INTAS (INTAS-Belarus Grant No. 97-0533).

References

1. Durnin J *J. Opt. Soc. Am. A* **2** 110 (1985); **4** 651 (1987)
2. Turunen J, Vasara A, Friberg A T *Appl. Opt.* **27** 3959 (1988)
3. Herman R M, Wiggins T A *J. Opt. Soc. Am. A* **8**, 932 (1991)
4. Davidson N, Friesem A A, Hasman E. *Opt. Commun.* **88** 326 (1992)
5. Andreev N E, Aristov Yu A, Polonskii L Ya, Pyatnitskii L N *Zh. Eksp. Teor. Fiz.* **100** 1765 (1991)
6. Wulle T, Herminghaus S *Phys. Rev. Lett.* **58** 1499 (1987)
7. Pandit M K, Payne F P *Opt. Quantum Electron.* **29** 35 (1997)
8. Shinozaki K, Xu Chang-ging, Sasaki H, Kamijoh T *Opt. Commun.* **133** 300 (1997)
9. Glushko B, Kryzhanovsky B, Sarkisyan D *Phys. Rev. Lett.* **71** 243 (1993)
10. Tewari S P, Huang H, Boyd R W *Phys. Rev. A* **71** R2707 (1995)
11. Caron C F R, Potwliege R M *J. Opt. Soc. Am. B.* **15** 1096 (1998)
12. Niggl L, Maier M *Opt. Lett.* **22** 910 (1997)
13. Piskarskas A P, Smilgevičius V, Stabinis A P *Appl. Opt.* **36** 7779 (1997)
14. Piskarskas A, Smilgevičius V, Stabinis A *Opt. Commun.* **143** 72 (1997)
15. Peet V E, Tsubin R V *Phys. Rev. A* **56** 1613 (1997)
16. Niggl L, Maier M *Opt. Commun.* **154** 65 (1998)
17. Klewitz S, Sogomonian S, Woerner M, Herminghaus S *Opt. Commun.* **154** 186 (1998)
18. Gadonas R, Marcinkevičius A, Piskarskas A, Smilgevičius V, Stabinis A *Opt. Commun.* **146** 253 (1998).
19. Belyi V N, Kazak N S, Kondratyuk N V, Khilo N A, Shagov A A *Kvantovaya Elektron.* **25** 1037 (1998) [*Quantum Electron.* **28**, 1011 (1998)]
20. Belyi V N, Kazak N S, Khilo N A, Shagov A A *Kvantovaya Elektron.* **25** 537 (1998) [*Quantum Electron.* **28**, 522 (1998)]
21. Gadonas R, Jarutis V, Marcinkevičius A, Smilgevičius V, Stabinis A *Opt. Commun.* **167** 299 (1999)
22. Belyi V N, Kazak N S, Khilo N A *Opt. Commun.* **162** 169 (1999)
23. Dmitriev V G, Gurzadyan G G, Nikogosyan D N *Handbook of nonlinear optical crystals* (Berlin, Springer-Verlag, 1999).
24. Günter P *Appl. Phys. Lett.* **34** 650 (1979)
25. Dmitriev V G, Tarasov L V *Prikladnaya Nelineinaya Optika* (Applied Nonlinear Optics) (Moscow: Radio i Svyaz', 1982, p. 123)

26. Danailov M B, Apai P, Belyi V N, Khilo N A, Kuzmin A N, Ryabtsev G I, Demidovich A A *III Intern. Winter Workshop on Spectroscopy and Structure of Rare Earth Systems* (Szklárska Poreba, 1999, p.9)
27. Baumert J C, Schellenberg F M, Lenth W, Risk W P, Bjorklund G C *Appl. Phys. Lett.* **51** 2192 (1987)
28. Khilo N A *Kvantovaya Elektron.* **30** 65 (2000) [*Quantum Electron.* **30** 65 (2000)]
29. Sukhorukov A P, Sukhorukova A K *Izv. Akad. Nauk RAS, Ser. Fiz.* **62** 2338 (1998)
30. Beržanskis A, Matijičsius A, Piskarskas A, Smilgevičius V, Stabinis A *Lithuanian J. Phys.* **37** 327 (1997)
31. Kazak N S, Khilo N A, Ryzhevich A A *Kvantovaya Elektron.* **29** 184 (1999) [*Quantum Electron.* **29**, 1020 (1999)]